inspired at all sampling sites at a height of 1.5 m above ground. An Andersen low-volume sampler was used to collect dust of various aerodynamic diameters to estimate the respirable portion of dust in Fukushima Prefecture. This sampler was fixed at a sampling site in Fukushima City. Dust samples were weighed, and their radioactivities were measured.

Determination of ^{137}Cs and ^{134}Cs

Aliquots of 100–200 g from each sample of food and cow's milk (dry weight), and soil (fresh weight) were weighed and sealed in cylindrical plastic containers. Filters from aerosol sampling were pressed into small cylindrical plastic containers. Radiometric determinations were performed using a high-purity, low-background, high-resolution germanium detector (0.7 keV). The detector was protected by a lead shield, 10 cm thick internally, covered with 0.5 mm electrolytic copper. A multichannel analyzer (4,096 channels, range 0–3,000 keV, MCA8000; Princeton Gamma Technologies, NJ, USA) was used for gamma-spectrum acquisition and processing. Characteristic gamma-ray energies were monitored to identify and quantify the radionuclides (^{134}Cs 604.7 and 795.9 keV, ^{137}Cs 661.7 keV). The detector was calibrated using a gamma-ray reference source from the Japan Radioisotope Association (Tokyo, Japan). The gamma spectrum of each sample was measured for >20,000 s for food and dust samples and for >2,000 s for soil samples. The lower limits of detection were 0.05 Bq/kg, 0.2 Bq/kg, 0.2 Bq/kg, 0.2 mBq/m^3, and 1 Bq/kg for food, vegetable, milk, dust, and soil samples, respectively. All samples were assumed to be in radioactive equilibrium. All activities were corrected to March 15, 2011 using physical half-lives (^{134}Cs 2.06 years, ^{137}Cs 30.1 years).

Effective dose coefficients for exposures by ingestion and inhalation

Radioactivities were converted into effective doses using effective dose coefficients of 0.019 μSv/Bq for ^{134}Cs and 0.013 μSv/Bq for ^{137}Cs by ingestion, respectively [7]. For inhalation, we assumed that a standard adult resident inhaled 20 m^3 air per day and used the effective dose coefficients of 0.02 μSv/Bq for ^{134}Cs and 0.039 μSv/Bq for ^{137}Cs for inhalation [7]. For the two routes of exposure, we postulated conservatively that all the radionuclides were retained in the body or in the lung, with no elimination.

Results and discussion

A total of 74 sets of whole-day meals were collected and analyzed. Their menus and components are presented in

Table 1 Dietary intake of radioactive cesium in Fukushima Prefecture

Sampling site	*n*		Food volume (g/day)	Water content (%)	Daily intake (Bq/day)		Estimated dose (μSv/year)
					^{134}Cs	^{137}Cs	
Fukushima total	55	*n* > MDL (%)	–	–	36 (65.5)	35 (63.6)	
		Median (range)	2,053 (1,100–3,145)	80.8 (73.3–97.6)	0.2 (ND–7.2)	0.3 (ND–7.0)	3.0 (ND–83.1)
		Mean ± SD	2,178 ± 400	81.9 ± 4.5	0.5 ± 1.1	0.6 ± 1.0	6.4 ± 12.5
Iwaki	10	*n* > MDL (%)	–	–	9 (90.0)	9 (90.0)	
		Median (range)	2,241 (1,879–2,690)	82.1 (76.8–86.1)	0.4 (ND–2.5)	0.7 (ND–1.6)	6.5 (ND–24.7)
		Mean ± SD	2,238 ± 272	81.5 ± 3.3	0.7 ± 0.8	0.7 ± 0.5	8.6 ± 7.8
Souma	10	*n* > MDL (%)	–	–	7 (70.0)	8 (80.0)	
		Median (range)	2,451 (2,044–2,795)	80.5 (73.3–87.1)	0.6 (ND–7.2)	0.9 (ND–7.0)	8.2 (ND–83.1)
		Mean ± SD	2,395 ± 293	80.1 ± 4.2	1.4 ± 2.2	1.6 ± 2.2	17.4 ± 25.3
Nihonmatsu	10	*n* > MDL (%)	–	–	5 (50.0)	4 (40.0)	
		Median (range)	2,611 (1,964–3,145)	79.4 (75.1–82.6)	0.1 (ND–0.9)	ND (ND–0.9)	1.7 (ND–10.4)
		Mean ± SD	2,529 ± 423	78.9 ± 2.3	0.3 ± 0.4	0.2 ± 0.3	2.9 ± 3.6
Fukushima	25	*n* > MDL (%)	–	–	15 (60.0)	14 (56.0)	
		Median (range)	1,954 (1,100–3,051)	83.7 (77.9–97.6)	0.1 (ND–0.8)	0.2 (ND–1.3)	1.3 (ND–11.3)
		Mean ± SD	1,927 ± 308	84.1 ± 4.8	0.2 ± 0.2	0.2 ± 0.3	2.6 ± 3.1
Kyoto (Uji)	19	*n* > MDL (%)	–	–	1 (5.3)	1 (5.3)	–
		Maximum	–	–	0.4	0.5	5.3
		Mean ± SD	2,955 ± 652	87.2 ± 2.5	–	–	–

Estimated dose is the total for doses attributable to exposure to ^{134}Cs and ^{137}Cs. The effective dose coefficients for ^{134}Cs and ^{137}Cs by oral route were 0.019 and 0.013 μSv/Bq, respectively

MDL method detection limit, *ND* less than MDL

Table 2 Radioactive cesium in local commercial products purchased in Fukushima Prefecture

Sampling site	*n*		Weight (g)	Radioactivity (Bq/kg)			Recommended standard[a] (Bq/kg)
				^{134}Cs	^{137}Cs	Total	
Milk							200
Fukushima total	21	$n >$ MDL (%)	–	20 (95.2)	19 (90.5)	–	
		Median (range)	–	1.8 (ND–4.9)	1.9 (ND–5.5)	4.1 (ND–10.1)	
		Mean ± SD	985 ± 119	2.1 ± 1.7	2.4 ± 1.9	4.5 ± 3.6	
Iwaki	3	$n >$ MDL (%)	–	3 (100.0)	3 (100)		
		Median (range)	–	0.9 (0.6–1.2)	1.2 (1.1–1.3)	2.0 (1.9–2.3)	
		Mean ± SD	752 ± 202	0.9 ± 0.3	1.2 ± 1.1	2.1 ± 0.2	
Souma	6	$n >$ MDL (%)	–	6 (100.0)	6 (100.0)	–	
		Median (range)	–	3.1 (1.4–3.8)	3.1 (1.9–4.4)	6.1 (3.3–8.2)	
		Mean ± SD	1,019 ± 29	2.8 ± 1.0	3.1 ± 1.0	5.9 ± 1.9	
Nihonmatsu	3	$n >$ MDL (%)	–	3 (100.0)	1 (33.3)		
		Median (range)	–	0.2 (0.2–1.3)	ND (ND–1.1)	0.2 (0.2–2.4)	
		Mean ± SD	1,047 ± 15	0.5 ± 0.7	0.4 ± 0.6	0.9 ± 1.3	
Fukushima	9	$n >$ MDL (%)	–	8 (88.9)	8 (88.9)	–	
		Median (range)	–	3.4 (ND–4.9)	3.9 (ND–5.5)	7.3 (0.2–10.1)	
		Mean ± SD	1,021 ± 18	2.6 ± 2.0	2.3 ± 4.4	5.6 ± 4.4	
Kyoto (Uji)	3	$n >$ MDL (%)	–	1 (33.3)	1 (33.3)	–	
		Median (range)	–	ND (ND–0.7)	ND (ND–0.7)	ND (ND–1.4)	
		Mean ± SD	1,037 ± 21	0.2 ± 0.4	0.2 ± 0.4	0.5 ± 0.8	

	Weight (g)	Radioactivity (Bq/kg weight)			Recommended standard[a] (Bq/kg)
		^{134}Cs	^{137}Cs	Total	
Vegetable/fruit					500
Kyoto (Uji)					
Spinach	1,249	ND	ND	ND	
Japanese mustard spinach	3,044	ND	ND	ND	
Fukushima (n = 43)					
Date					
Japanese mustard spinach	1,828	2.6	2.2	4.8	
Spinach	1,677	0.2	0.3	0.5	
New Zealand spinach	1,097	29.9	32.7	62.6	
Ceylon spinach	826	2.1	3.1	5.2	
Cucumber	1,643	3.4	4.5	7.9	
Welsh onion	1,770	3.3	2.8	6.1	
Kawamata					
Mizuna	504	5.9	7.7	13.7	
Shiitake	1,012	140.4	164.2	304.6	
Ceylon spinach	503	4.4	3.0	7.4	
Cucumber	1,007	1.3	1.6	2.8	
Broccoli	831	6.4	6.6	12.9	
Chinese chives	704	7.2	4.5	11.7	
Partially dried Japanese persimmon	332	1.8	1.7	3.5	
Welsh onion	1,455	5.7	6.6	12.3	
Fukushima					
Chinese chives	436	1.9	2.0	3.9	
Cucumber	493	2.9	3.9	6.8	

Table 2 continued

	Weight (g)	Radioactivity (Bq/kg weight)			Recommended standard[a] (Bq/kg)
		^{134}Cs	^{137}Cs	Total	
Iwaki					
Spinach	1,903	0.5	0.9	1.4	
Snap bean	860	3.5	3.6	7.1	
Shiitake	89	ND	ND	ND	
Green onion	571	7.3	8.5	15.8	
Chinese chives	615	2.8	3.5	6.3	
Broccoli	1,479	0.9	1.1	2.0	
Ceylon spinach	1,079	1.5	2.6	4.0	
Garlic	691	0.8	0.5	1.3	
Souma					
Welsh onion	1,543	4.1	2.6	6.7	
Peach	794	9.3	7.9	17.2	
Cherry	244	29.3	37.3	66.6	
Broad beans	418	4.9	6.0	10.9	
Onion (large)	835	0.5	0.6	1.1	
Onion (small)	430	9.1	9.2	18.3	
Red onion (large)	589	3.3	5.0	8.3	
Red onion (small)	524	9.6	11.6	21.3	
Garlic	256	9.4	7.2	16.6	
Potato	1,258	1.0	0.8	1.8	
Minamisouma					
Carrot	1,271	1.4	2.1	3.5	
Shiitake	417	127.1	154.7	281.8	
Bell pepper	502	ND	ND	ND	
Nihonmatsu					
Asparagus	637	1.3	1.5	2.8	
Bell pepper	390	12.0	10.7	22.7	
Ceylon spinach	1,533	1.7	3.2	4.9	
Cucumber	2,064	3.6	4.3	7.9	
Welsh onion	1,309	5.4	5.0	10.5	
Cherry	352	24.5	28.5	52.9	

MDL method detection limit, *ND* less than MDL

[a] Recommended by Ministry of Health, Labor, and Welfare of Japan [8]

Table S1. Radioactivity per daily intake (Bq/day) is also summarized in Table 1. ^{134}Cs or ^{137}Cs was detected in 36 of 55 whole-day meal samples from Fukushima Prefecture, compared with only one of 19 from Kyoto. The estimated median dose levels was 3.0 μSv/year, ranging from not detectable (ND) to 83.1 μSv/year in Fukushima, while the maximum dose level in Kyoto was 5.3 μSv/year.

The levels of ^{134}Cs and ^{137}Cs in cow's milk and vegetables were also determined (Table 2). The median total activity in milk from Fukushima Prefecture was 4.1 Bq/kg, ranging from ND to 10.1, which was an order of magnitude lower than the recommended limit set by the Ministry of Health, Labor, and Welfare of Japan [8]. Trace radioactivity was detected in only one sample from Kyoto. No vegetables in Fukushima Prefecture exceeded 100 Bq/kg, except for shiitake mushrooms (*Lentinula edodes*), which contained relatively high levels of radioactivity, up to 60% of the recommended limit (Table 2). Radioactivities in shiitake at Kawamata or Minamisouma were larger than at Iwaki, indicating that a radioactive plume was transferred by northeasterly winds from the nuclear plant. No radioactivity was detected in vegetables from Kyoto. These results indicate that the levels of radioactive Cs ingested were well below the recommended limits [8] in various towns in Fukushima Prefecture, except in the case of shiitake.

Table 3 Particle size distribution and respiratory deposition estimate for radioactive cesium in Fukushima Prefecture

Sampling site		Date (2011)	Andersen low-volume sampler, 224 m^3			
			Fraction (μm)	Dust amount (mg)	Radioactivity (mBq/m^3-air)	
					^{134}Cs	^{137}Cs
Fukushima	37°45′42″N 140°28′18″E	7/2–7/8	100–11.4	0.7	0.4	0.3
			11.4–7.4	1.1	0.3	0.3
			7.4–4.9	1	1.0	0.4
			4.9–3.3	0.9	0.5	0.6
			3.3–2.2	0.6	0.3	0.2
			2.2–1.1	0.8	0.3	0.2
			1.1–0.7	1.3	0.8	0.4
			0.7–0.46	1.3	1.5	1.1
			<0.46	0.9	1.5	1.3
		Total		8.6	6.5	4.7
		Respirable	<4.9	5.8	4.8	3.8

Sampling site		Date (2011) (weather)	High-volume air sampler							Ambient dose rate	Radioactivity in soil (Bq/kg)		
			Air volume sampled (m^3)	Dust amount (mg)	Radioactivity in air (mBq/m^3-air)		Estimated dose[a] (μSv/year)						
					^{134}Cs	^{137}Cs	^{134}Cs	^{137}Cs	Total	(μSv/h)	^{134}Cs	^{137}Cs	*n*
Fukushima	37°45′42″N 140°28′18″E	2011/7/2 (F)	473	6.8	1.9	3.0	0.3	0.8	1.1	1.2	NA	NA	
Date	37°47′10″N 140°33′26″E	2011/7/3 (CL)	94	3.5	7.9	6.4	1.1	1.8	3.0	0.9	3,232 ± 2,666	3,855 ± 3,047	5
Fukushima	37°39′26″N 140°32′11″E	2011/7/3 (CL)	83	1.9	4.7	1.5	0.7	0.4	1.1	1.0	2,515 ± 859	3,059 ± 1,077	5
Fukushima	37°45′42″N 140°28′18″E	2011/7/4 (R)	450	8	1.6	1.5	0.2	0.4	0.6	1.2	NA	NA	
Souma	37°46′1″N 140°57′2″E	2011/7/5 (F)	88	0.7	0.6	0.2	0.1	0.1	0.1	0.5	1,710 ± 2,365	2,116 ± 2,976	5
Minami-Souma	37°38′29″N 140°55′30″E	2011/7/5 (F)	84	2.4	0.7	1.1	0.1	0.3	0.4	0.9	1,772 ± 411	2,151 ± 546	5
Souma	37°46′8″N 140°43′1″E	2011/7/5 (F)	84	1.3	1.1	2.3	0.2	0.7	0.8	1.6	1,723 ± 1,792	2,047 ± 2,174	5
Fukushima	37°45′42″N 140°28′18″E	2011/7/5 (F)	220	4	2.9	3.4	0.4	1.0	1.4	1.2	NA	NA	
Nihonmatsu	37°33′21″N 140°27′34″E	2011/7/6 (F)	93	0.1	0.6	0.6	0.1	0.2	0.3	1.2	12,184 ± 12,170	14,202 ± 14,025	5
Nihonmatsu	37°33′21″N 140°30′43″E	2011/7/6 (F)	53	0.3	4.2	7.3	0.6	2.1	2.7	1.9	1,895 ± 674	2,244 ± 755	5
Kawamata	37°36′14″N 140°38′49″E	2011/7/6 (CL)	72	0.4	6.3	6.1	0.9	1.7	2.7	2.0	3,931 ± 4,856	4,741 ± 5,929	5
Fukushima	37°45′42″N 140°28′18″E	2011/7/6 (CL)	246	4	5.3	7.6	0.8	2.2	2.9	1.2	NA	NA	
Fukushima	37°45′42″N 140°28′18″E	2011/7/7 (CL)	259	5.3	1.9	2.5	0.3	0.7	1.0	1.2	NA	NA	
Iitate	37°36′44″N 140°44′52″E	2011/7/7 (CL)	84	1.7	24.6	38.9	3.6	11.1	14.7	9.0	18,531 ± 11,235	23,185 ± 15,664	5
Namie	37°33′38″N 140°45′39″E	2011/7/7 (CL)	84	1.7	148.2	194.2	21.6	55.3	76.9	13.0	13,548 ± 10,469	16,216 ± 12,653	5
Katsurao	37°31′33″N 140°48′21″E	2011/7/7 (CL)	84	1.5	65.0	64.0	9.5	18.2	27.7	10.0	16,332 ± 11,170	16,799 ± 10,058	5

CL cloudy, *F* fine, *R* rainy, *NA* not available

[a] It was assumed that radioactive cesium was in respirable fraction and that a standard human inhales 20 m^3 air

We collected 16 dust samples using the high-volume sampler (Table 3; Fig. 1). Data obtained with the low-flow-volume sampler suggested that a large proportion of the radionuclides from the crippled Fukushima nuclear power plant was in the respirable fraction: 74% (4.8/6.5) of the total ^{134}Cs and 81% (3.8/4.7) of the total ^{137}Cs (Table 3). To estimate the exposure doses for humans, we therefore selected a conservative scenario whereby all ^{134}Cs and ^{137}Cs activities in the dust samples collected using the high-volume sampler were allocated to the respirable fraction (aerodynamic diameter <4.9 μm). The highest dose level of 76.9 μSv/year was recorded in a sample collected at Namie. However, this value was still less than one-tenth of the permissible dose level of 1 mSv/year [8]. The estimated dose levels for ^{137}Cs were significantly correlated with ambient dose rate (μSv/h) ($n = 10$, $r^2 = 0.79$, $p < 0.05$) but not with mean radioactivity levels in soil (Bq/kg) ($n = 11$, $r^2 = 0.32$, $p > 0.05$).

Given that the samples in this study were obtained in early July, about 4 months after the major release of radioactivity, airborne radioactivity was likely to represent resuspended deposited radioactivity, rather than direct transport from the source. Several studies have investigated resuspension from a flat surface [5], but information on resuspension from ecological systems including forests and paddy fields is scant.

We demonstrated the radioactivity levels due to ^{134}Cs and ^{137}Cs in Fukushima Prefecture in July 2011. The maximum total exposure dose through inhalation and ingestion was estimated to be 160 μSv/year (83.1 by ingestion and 76.9 by inhalation) in zones outside a 20-km radius of the crippled Fukushima nuclear power plant.

The amounts of radioactivity in the daily meals consumed by residents of the study regions were well below the regulation limit. However, many food items are now imported globally, such that a high portion of foodstuffs comes from uncontaminated areas. It is possible that the radioactivity in some highly contaminated foodstuffs may be diluted by other "clean" foods. However, the ingested doses estimated in the present study would underestimate the exposure of residents whose daily foods are mostly supplied locally from within the contaminated areas. The conclusions of this study may therefore not be applicable to people in such a situation. Furthermore, the current study only utilized air monitoring in a few, geographically limited areas. All meal samples were obtained from outside a 30-km radius of the nuclear power plant, because no commercial venders were present between 20 and 30 km from the power plant, which had been defined as the planned emergency evacuation zone. In addition to the small number of air samples collected, the survey was conducted in the rainy season when "resuspension" is relatively low. The current study is thus subject to the above limitations and biases. However, the conservative approach adopted in this study maximized the estimated dose levels and would thus partially mitigate the effects of any biases and limitations. In conclusion, the estimated dose levels in residents of Fukushima Prefecture as a result of ingestion and inhalation were much lower than the 1 mSv/year, recognized as a publicly permissible dose [8]. Further studies are needed to perform qualitative risk assessments based on more accurate exposure estimates.

Acknowledgments This study was supported by a Grant-in-Aid for Health Sciences Research from the Ministry of Health, Labor, and Welfare of Japan (H21-Food-003), an urgent collaborative research grant from the Disaster Prevention Research Institute, Kyoto University (23U-01), and Tokyo Kenbikyoin Foundation.

Conflicts of interest The authors declare that there are no conflicts of interest.

References

1. Fukushima radioactive fallout nears Chernobyl levels. Newscientist.com. 2011. http://www.newscientist.com/article/dn20285-fukushima-radioactive-fallout-nears-chernobyl-levels.html. Accessed 24 Apr 2011.
2. Peter Grier. Was Chernobyl really worse than Fukushima? The Christian Science Monitor. 2011. http://www.csmonitor.com/USA/2011/0426/Was-Chernobyl-really-worse-than-Fukushima. Accessed 26 Apr 2011.
3. Chino M, Nakayama H, Nagai H, Terada H, Katata G, Yamazawa H. Preliminary estimation of release amounts of ^{131}I and ^{137}Cs accidentally discharged from the Fukushima Daiichi nuclear power plant into the atmosphere. J Nucl Sci Tech. 2011;48:1129–34.
4. Tsuji M, Kanda H, Kakamu T, Kobayashi D, Miyake M, Hayakawa T, Mori Y, Okochi T, Hazama A, Fukushima T. An assessment of radiation doses at an educational institution 57.8 km away from the Fukushima Daiichi nuclear power plant 1 month after the nuclear accident. Environ Health Prev Med. 2011. doi: 10.1007/s12199-011-0229-7.
5. Ishikawa H. Evaluation of the effect of horizontal diffusion on the long-range atmospheric transport simulation in Chernobyl data. J Appl Meteorol. 1995;34:1653–65.
6. Koizumi A, Harada KH, Inoue K, Hitomi T, Yang HR, Moon CS, Wang P, Hung NN, Watanabe T, Shimbo S, Ikeda M. Past, present, and future of environmental specimen banks. Environ Health Prev Med. 2009;14:307–18.
7. International Commission on Radiological Protection (ICRP). Age-dependent doses to the members of the public from intake of radionuclides—part 5 compilation of ingestion and inhalation coefficients. ICRP Publication 72. Ann ICRP. 1995;26(1).
8. Department of Food Safety, Ministry of Health, Labour and Welfare. Handling of food contaminated by radioactivity (Relating to the accident at the Fukushima Nuclear Power Plant). March 17, 2011. http://www.mhlw.go.jp/stf/houdou/2r9852000001558e-img/2r98520000015apy.pdf and http://www.mhlw.go.jp/stf/houdou/2r9852000001558e-img/2r98520000015av4.pdf

Circulation
JOURNAL OF THE AMERICAN HEART ASSOCIATION

American Heart Association®
Learn and Live℠

Blockade of the Nuclear Factor-κB Pathway in the Endothelium Prevents Insulin Resistance and Prolongs Life Spans

Yutaka Hasegawa, Tokuo Saito, Takehide Ogihara, Yasushi Ishigaki, Tetsuya Yamada, Junta Imai, Kenji Uno, Junhong Gao, Keizo Kaneko, Tatsuo Shimosawa, Tomoichiro Asano, Toshiro Fujita, Yoshitomo Oka and Hideki Katagiri

Circulation 2012, 125:1122-1133: originally published online February 1, 2012
doi: 10.1161/CIRCULATIONAHA.111.054346
Circulation is published by the American Heart Association. 7272 Greenville Avenue, Dallas, TX 72514
 Print ISSN: 0009-7322. Online ISSN: 1524-4539

Blockade of the Nuclear Factor-κB Pathway in the Endothelium Prevents Insulin Resistance and Prolongs Life Spans

Yutaka Hasegawa, MD, PhD*; Tokuo Saito, MD, PhD*; Takehide Ogihara, MD, PhD; Yasushi Ishigaki, MD, PhD; Tetsuya Yamada, MD, PhD; Junta Imai, MD, PhD; Kenji Uno, MD, PhD; Junhong Gao, MD, PhD; Keizo Kaneko, MD, PhD; Tatsuo Shimosawa, MD, PhD; Tomoichiro Asano, MD, PhD; Toshiro Fujita, MD, PhD; Yoshitomo Oka, MD, PhD; Hideki Katagiri, MD, PhD

Background—Nuclear factor-κB (NF-κB) signaling plays critical roles in physiological and pathological processes such as responses to inflammation and oxidative stress.

Methods and Results—To examine the role of endothelial NF-κB signaling in vivo, we generated transgenic mice expressing dominant-negative IκB under the Tie2 promoter/enhancer (E-DNIκB mice). These mice exhibited functional inhibition of NF-κB signaling specifically in endothelial cells. Although E-DNIκB mice displayed no overt phenotypic changes when young and lean, they were protected from the development of insulin resistance associated with obesity, whether diet- or genetics-induced. Obesity-induced macrophage infiltration into adipose tissue and plasma oxidative stress markers were decreased and blood flow and mitochondrial content in muscle and active-phase locomotor activity were increased in E-DNIκB mice. In addition to inhibition of obesity-related metabolic deteriorations, blockade of endothelial NF-κB signaling prevented age-related insulin resistance and vascular senescence and, notably, prolonged life span. These antiaging phenotypes were also associated with decreased oxidative stress markers, increased muscle blood flow, enhanced active-phase locomotor activity, and aortic upregulation of mitochondrial sirtuin-related proteins.

Conclusions—The endothelium plays important roles in obesity- and age-related disorders through intracellular NF-κB signaling, thereby ultimately affecting life span. Endothelial NF-κB signaling is a potential target for treating the metabolic syndrome and for antiaging strategies. (***Circulation.*** **2012;125:1122-1133.)**

Key Words: inflammation ■ insulin resistance ■ oxidative stress ■ NF-κB

Nuclear factor-kappa B (NF-κB) is a transcription factor regulating the gene expression of numerous cytokines, growth factors, adhesion molecules, and enzymes involved in a variety of pivotal cellular processes, including responses to inflammation and oxidative stress.[1] Without inflammatory stimuli, NF-κB is maintained in the cytoplasm in a nonactivated form by association with an inhibitor subunit, IκB. In response to activating stimuli, including tumor necrosis factor-α (TNF-α), lipopolysaccharide, and other inflammatory cytokines, IκB is phosphorylated by IκB kinase β, resulting in proteolysis of IκB. Consequently, a nuclear recognition site of NF-κB is exposed, and NF-κB is stimulated to move into the nucleus, resulting in mRNA expression of target genes, including inflammatory cytokines and adhesion molecules.[2]

Editorial see p 1081
Clinical Perspective on p 1133

Obesity is characterized by a state of chronic low-grade inflammation.[3] Oxidative stress is also widely recognized as being associated with various obesity-related disorders.[4] Insulin resistance is an important mechanism underlying obesity-related disorders, eg, diabetes mellitus, hyperlipidemia, and hypertension, collectively called the metabolic syndrome.[5,6] In these metabolic states, NF-κB has been implicated in the processes of both inflammatory responses

Received January 12, 2011; accepted December 27, 2011.

From Division of Molecular Metabolism and Diabetes (Y.H., T. Saito, Y.I., J.I., K.U., K.K., Y.O.) and Department of Metabolic Diseases, Center for Metabolic Diseases (T. Saito, T.O., T.Y., J.G., H.K.), Tohoku University Graduate School of Medicine, Sendai; Faculty of Medicine, Department of Clinical Laboratory (T. Shimosawa) and Department of Nephrology and Endocrinology, Faculty of Medicine (T.F.), University of Tokyo, Tokyo; and Department of Medical Science, Graduate School of Medicine, University of Hiroshima, Hiroshima (T.A.), Japan.

*Drs Hasegawa and Saito contributed equally to this article.

The online-only Data Supplement is available with this article at http://circ.ahajournals.org/lookup/suppl/doi:10.1161/CIRCULATIONAHA.111.054346/-/DC1.

Correspondence to Hideki Katagiri, MD, PhD, Department of Metabolic Diseases, Center for Metabolic Diseases, Tohoku University Graduate School of Medicine, 2-1 Seiryo-machi, Aoba-ku, Sendai 980-8575, Japan. E-mail katagiri@med.tohoku.ac.jp

Circulation **is available at http://circ.ahajournals.org** **DOI: 10.1161/CIRCULATIONAHA.111.054346**

and oxidative stress.[7] Indeed, blockade of the NF-κB signaling pathway by systemic administration of high-dose salicylate or global disruption of IκB kinase β reportedly suppresses inflammatory processes associated with insulin resistance in obesity and type 2 diabetes mellitus.[8,9] However, the sites at which the NF-κB signaling pathway plays critical roles in these pathological processes remain to be elucidated.

The endothelium lines the entire vascular system in a single cell layer, forming an interface between vascular structures and blood. In human adults, ≈10 trillion (10^{13}) cells form an almost 1-kg organ. Endothelial cells produce and react to a wide variety of inflammation-related mediators such as cytokines, growth factors, and adhesion molecules.[10] Endothelial injury and dysfunction are involved in the development of many diseases, including vascular diseases and inflammatory disorders.[11,12] In this context, we hypothesized that NF-κB signaling in endothelial cells contributes to obesity-related disorders. Furthermore, insulin resistance and increased oxidative stress also are commonly observed in aged states. Therefore, we also hypothesized that endothelial proinflammatory responses play important roles in age-related disorders, ultimately affecting life span. Here, using the transgenic technique, we show that blockade of the intracellular NF-κB pathway in the endothelium prevents obesity- and age-related insulin resistance and enhances longevity.

Methods

Animals

Animal studies were conducted in accordance with the institutional guidelines for animal experiments at Tohoku University. The mutant cDNA for human IκBα, with alanine substitutions of 2 serine residues (32 and 36), was cloned into a transgenic vector, pSPTg.T2FpAXK, provided by Thomas N. Sato. This vector contains the Tie2 promoter, SV40 polyA signal, and Tie2 minimum enhancer fragment (Figure 1A). E-DNIκB;A^y/+ mice were obtained by mating male KK A^y (A^y/+) mice (Nippon CLEA, Shizuoka, Japan), a genetic model for obesity-diabetes syndrome, and female E-DNIκB mice. E-DNIκB mice were also crossed with endothelial nitric oxide (NO) synthase (eNOS)–deficient ($Nos3^{-/-}$) mice with the C57BL/6J background[13] to generate E-DNIκB;$Nos3^{-/-}$ mice.

Blood analysis, glucose tolerance tests, insulin tolerance tests, histological analysis, oxygen consumption, and locomotor activity were performed as described[14] in the online-only Data Supplement.

Isolation and Culture of Endothelial Cells

Endothelial cells were isolated from murine lung with a MACS separation unit (Miltenyi Biotec, Surry, UK) as previously described.[15] To quantify vascular cell adhesion molecule-1 (VCAM-1) expression, purified endothelial cells were preincubated for 1 hour and then stimulated with or without TNF-α (10 ng/mL) for 4 hours, followed by quantitative reverse-transcriptase polymerase chain reaction analysis.

Hyperinsulinemic-Euglycemic Clamp

Hyperinsulinemic-euglycemic clamp studies were performed as described previously.[16] Details of the method are given in the online-only Data Supplement.

Blood Pressure Measurement

Systolic blood pressure in the conscious state was measured by the indirect tail cuff method with a model MK-2000 BP monitor (Muromachi Kikai, Tokyo, Japan) according to the manufacturer's instructions.[17] At least 6 readings were obtained for each experiment, and a mean value was assigned to each individual mouse.

Muscle Blood Flow Measurement

Muscle blood flow was measured with the fluorescent microsphere method as previously described.[18] Details of the method are given in the online-only Data Supplement.

Histological Analysis

Tissues sections were prepared and analyzed as described in the online-only Data Supplement. Total adipocyte areas were traced manually and analyzed. White adipocyte areas were measured in ≥100 cells per mouse in each group as described previously.[19]

Detection of Cellular Senescence

Cellular senescence was evaluated by senescence-associated β-galactosidase staining. Senescence-associated β-galactosidase was detected with a senescence detection kit (BioVision, Milpitas, CA) as previously described.[20] Senescence-associated β-galactosidase–positive areas were quantified by Easy Access (AD Science Co, Chiba, Japan).

Statistical Analysis

All data are expressed as mean±SEM. Images shown are representative of data from >3 independent experiments. All statistical analyses were performed with Ekuseru-Tokei 2010 statistical software (Social Survey Research Information Co, Ltd, Tokyo, Japan). Normality was tested with the Kolmogorov-Smirnov test. When data were normally distributed, the statistical significance of differences was assessed by 1-way ANOVA. Multiple experimental groups were compared by use of a Bonferroni test. Data were analyzed with nonparametric ANOVA (Kruskal-Wallis) when conformity to a normal distribution was not confirmed. Repeated-measures ANOVA was used to compare data obtained by serial measurements over time between the 2 experimental groups. Survival rates were compared between E-DNIκB mice and control littermates by the Kaplan-Meier method with log-rank tests. In all analyses, values of $P<0.05$ were accepted as statistically significant.

The authors had full access to and take full responsibility for the integrity of the data. All authors have read and agree to the manuscript as written.

Results

Construction of the Transgene and Generation of the E-DNIκB Mice

To block the NF-κB signaling in endothelial cells, we generated transgenic mice (E-DNIκB mice) in which the dominant-negative form of human IκBα (DNIκBα), with alanine substitutions of 2 serine residues (32 and 36), was expressed under the control of the Tie2 enhancer/promoter (Figure 1A). Immunoblotting of lung lysates confirmed the expression of transgene-derived human IκBα, ie, DNIκBα, with a slightly higher molecular weight than the murine, ie, endogenous, IκBα protein (Figure 1B). Transgene expression was apparent in the lung, in which the endothelium is abundant, but was only faintly detectable in other tissues such as the liver, pancreas, muscle, and adipose tissue (Figure 1B). In addition, endogenous IκBα proteins were degraded whereas DNIκBα remained essentially intact without degradation after TNF-α stimulation (Figure 1C). Immunostaining of lung tissue revealed that movement of NF-κB to the nucleus in response to TNF-α stimulation was markedly inhibited by DNIκBα expression (Figure 1D).

To further confirm the functional inhibition of endothelial NF-κB signaling, we isolated endothelial cells from murine

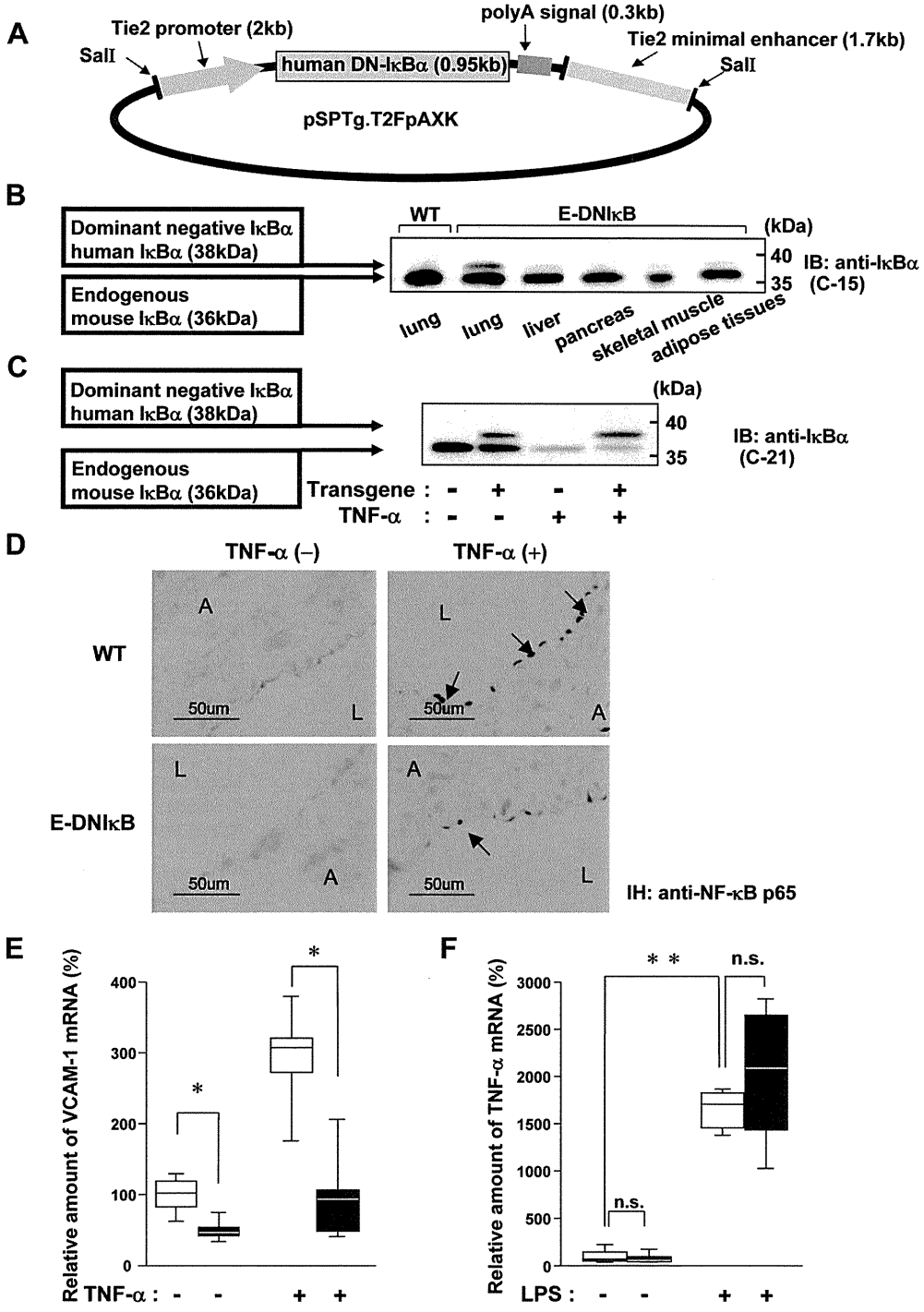

Figure 1. Generation of endothelial dominant-negative IκBα transgenic (E-DNIκB) mice. **A**, The construct of the transgene for generating E-DNIκB mice. **B**, Extracts of various tissues, as indicated, obtained from control and E-DNIκB mice were immunoblotted with anti-IκBα antibody. Exogenous (human) IκBα has a slightly higher molecular weight than endogenous (murine) IκBα. WT indicates wild type. **C**, Lung extracts of nontransgenic (control) and E-DNIκB mice were obtained 30 minutes after injection of tumor necrosis factor-α (TNF-α; 25 μg/kg), followed by immunoblotting with anti-IκBα antibody. **D**, Sections of thoracic aortas obtained from control and E-DNIκB mice were immunostained with anti-p65 (nuclear factor-κB [NF-κB] subunit) antibody. L indicates lumen; A, adventitia. Arrows indicate endothelial nuclei. **E**, Endothelial cells were isolated from lungs of control (white bars) and E-DNIκB (black bars) mice (n=6 per group) by use of a MACS separation unit. Purified endothelial cells were stimulated with or without TNF-α (10 ng/mL) for 4 hours, followed by analysis of vascular cell adhesion molecule-1 (VCAM-1) expression by quantitative reverse-transcriptase polymerase chain reaction (RT-PCR). **F**, Circulating blood cells from control (white bars) and E-DNIκB (black bars) mice (n=5 per group) were stimulated with or without lipopolysaccharide (100 ng/mL) for 3 hours, followed by analysis of TNF-α expression by quantitative RT-PCR analysis. In **E** and **F**, the relative amounts of mRNA were calculated with β-actin mRNA as the invariant control. Data are presented as mean±SEM. *$P<0.05$, **$P<0.01$ by 1-way ANOVA and Kruskal-Wallis tests.

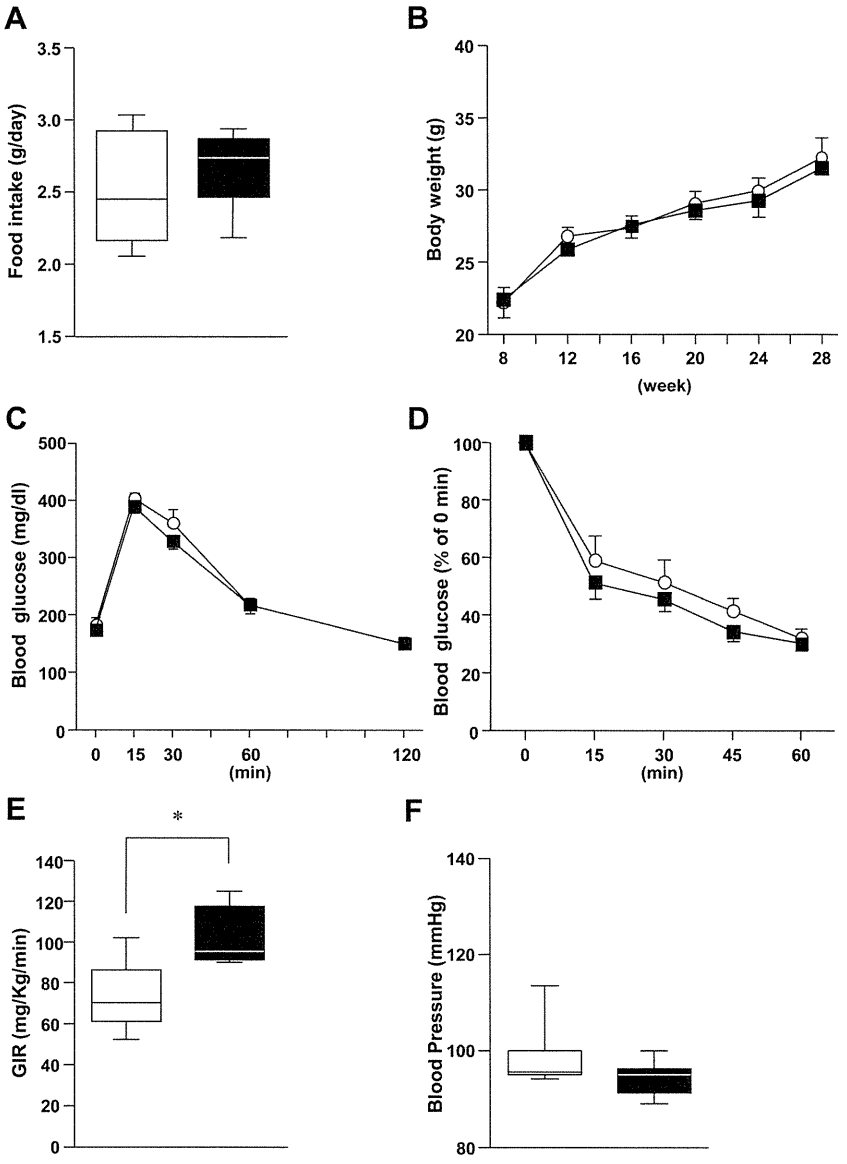

Figure 2. Young endothelial dominant-negative IκBα transgenic (E-DNIκB) mice showed no apparent phenotypic differences. **A**, Control (white bars) and E-DNIκB (black bars) mice were maintained on a normal chow diet, and food intake was measured at 8 weeks of age. **B**, Body weights of control (○) and E-DNIκB (■) mice maintained on a normal chow diet were measured weekly from 8 to 28 weeks of age. **C**, Glucose tolerance tests were performed with a peritoneal glucose load (2 g/kg body weight) after a 10-hour fast at 8 weeks of age. **D**, Insulin tolerance tests were performed in an ad libitum–fed state. Data are expressed as percentages of blood glucose levels immediately before intraperitoneal insulin loading (0.25 U/kg body weight). **E**, Hyperinsulinemic-euglycemic clamp tests were performed in control (white bars, n=4) and E-DNIκB (black bars, n=4) mice at 8 weeks of age, and glucose infusion rate (GIR) was calculated. **F**, Systolic blood pressures of control and E-DNIκB mice were measured at 8 weeks of age. Data are presented as mean±SEM. n=5 in control and n=6 in E-DNIκB mice. *$P<0.05$ by 1-way and repeated-measures ANOVA.

lung and analyzed the expression of VCAM-1, a target gene of NF-κB.[21] In isolated endothelial cells from wild-type mice, TNF-α upregulated VCAM-1 expression, whereas basal and TNF-α–induced VCAM-1 expression was markedly inhibited in isolated endothelial cells from E-DNIκB mice (Figure 1E). In contrast, in circulating cells from E-DNIκB mice, neither basal nor lipopolysaccharide-induced TNF-α expression was suppressed (Figure 1F). These findings demonstrate that NF-κB signaling is functionally blocked specifically in endothelial cells of the E-DNIκB mice used in this study.

Young E-DNIκB Mice Showed No Apparent Phenotypic Differences Compared With Control Mice

First, we analyzed glucose metabolism in these mice on a normal chow diet at 8 weeks of age. Food intakes (Figure 2A) and body weights (Figure 2B) were similar in E-DNIκB mice and their wild-type littermate controls. Glucose tolerance tests revealed no significant differences in blood glucose levels before and after glucose loading between these 2 groups (Figure 2C). In addition, blood glucose levels on insulin tolerance tests did not differ significantly between these 2 groups (Figure 2D). In contrast, a hyperinsulinemic-euglycemic clamp study, a more sensitive procedure for estimating insulin sensitivity, showed increased glucose infusion rates in E-DNIκB mice (Figure 2E). Because hyperinsulinemia during the clamp procedure suppresses hepatic glucose production, these findings indicate slight improvement of insulin sensitivity in insulin-responsive tissues, mainly muscle. Furthermore, systolic blood pressure was also similar in these 2 groups (Figure 2F). Thus, although young and on a normal chow diet, E-DNIκB mice showed no apparent phenotypic differences from control mice, except for slightly improved insulin sensitivity.

E-DNIκB Mice Were Protected From Obesity-Induced Insulin Resistance

We next analyzed the effects of endothelial NF-κB signaling blockade on glucose metabolism and insulin sensitivity in

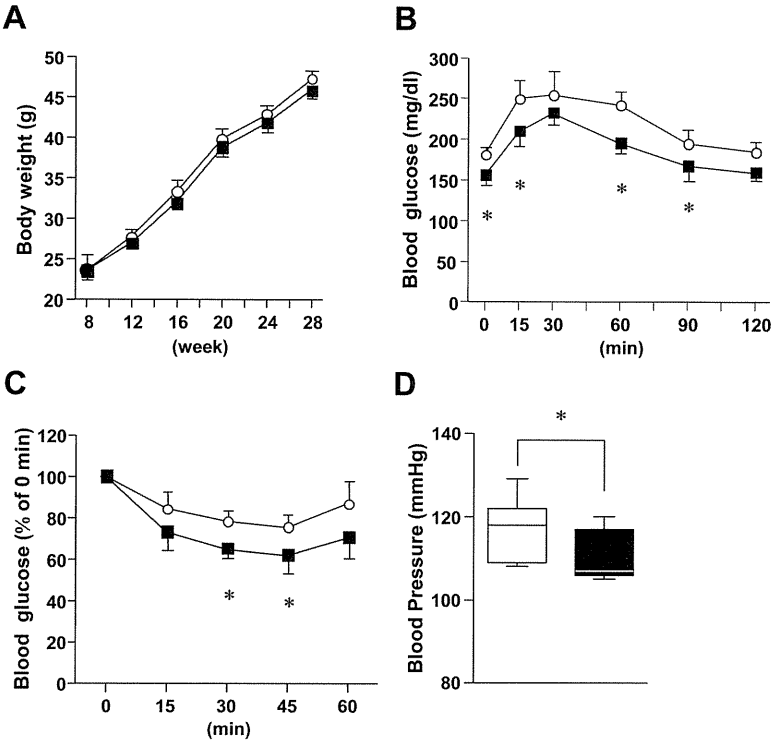

Figure 3. Endothelial dominant-negative IκBα transgenic (E-DNIκB) mice are protected from high-fat diet–induced obesity and insulin resistance. **A**, Body weights of control (○) and E-DNIκB (■) mice maintained on a high-fat diet were measured weekly from 8 to 28 weeks of age. **B**, Glucose tolerance tests were performed with a peritoneal glucose load (0.5 g/kg body weight) after a 10-hour fast in mice maintained on a high-fat diet at 28 weeks of age. **C**, Insulin tolerance tests were performed in an ad libitum–fed state. Data are expressed as percentages of blood glucose levels immediately before intraperitoneal insulin loading (0.8 U/kg body weight) in mice maintained on a high-fat diet at 28 weeks of age. **D**, Systolic blood pressures of control (white bars) and E-DNIκB (black bars) mice maintained on a high-fat diet at 24 to 28 weeks of age. Data are presented as mean±SEM. n=6 in control and n=7 in E-DNIκB mice. *$P<0.05$ by 1-way and repeated-measures ANOVAs.

states of obesity. First, E-DNIκB mice with the C57BL/6J background were placed on a high-fat diet starting from 8 weeks of age. Body weights were similarly increased in E-DNIκB mice and their wild-type littermate controls (Figure 3A). However, after 20 weeks of high-fat loading, differences in glucose tolerance and insulin sensitivity became evident. Glucose and insulin tolerance tests revealed that blockade of endothelial NF-κB signaling significantly protected these mice from the development of glucose intolerance (Figure 3B) and insulin resistance (Figure 3C). Furthermore, systolic blood pressure was significantly lower in E-DNIκB mice (Figure 3D). These findings indicate that inhibition of endothelial NF-κB signaling prevents obesity-induced disorders such as insulin resistance, glucose intolerance, and hypertension.

The prevention of insulin resistance and hypertension achieved by inhibiting endothelial NF-κB signaling was observed in genetically obese ($A^y/+$) mice in earlier periods. Body weights were slightly lower in E-DNIκB;$A^y/+$ than in control littermate $A^y/+$ mice at 16 weeks of age (Figure I in the online-only Data Supplement). Glucose (Figure 4A) and insulin (Figure 4B) tolerance tests revealed markedly better glucose tolerance and insulin sensitivity with blockade of endothelial NF-κB signaling. In contrast, hepatic expression of gluconeogenic genes, phosphoenolpyruvate carboxykinase, and glucose-6-phosphatase did not differ significantly between the 2 groups (Figure II in the online-only Data Supplement), suggesting that muscle is the major tissue responsible for improvement of insulin sensitivity achieved by blockade of endothelial NF-κB signaling. Systolic blood pressure was also significantly lower in E-DNIκB;$A^y/+$ mice than in $A^y/+$ littermates (Figure 4C). In addition, aortic expression of adhesion molecules such as VCAM-1 and E-selectin was decreased in E-DNIκB;$A^y/+$ mice (Figure 4D). Simultaneously, eNOS expression was significantly increased (Figure 4D), which may have contributed to the lower blood pressures.

Obesity-Associated Macrophage Infiltration Into Adipose Tissue Was Markedly Inhibited in E-DNIκB Mice

Obesity is a chronic state of low-grade inflammation leading to insulin resistance and oxidative stress. Macrophage infiltration into white adipose tissue reportedly contributes to the underlying mechanism.[22,23] Therefore, we histologically analyzed white adipose tissue, an important site of obesity-related inflammation. The adipocyte sizes and weights of epididymal fat tissue were smaller in E-DNIκB;$A^y/+$ mice than in control $A^y/+$ littermates, whereas liver weights did not differ significantly (Figure 4E and Figure I in the online-only Data Supplement). These findings suggest that less adiposity contributes to the better glucose tolerance in E-DNIκB;$A^y/+$ mice. Although immunohistochemical staining with antibodies against MOMA-2, a macrophage marker, revealed massive infiltration of macrophages into adipose tissue in $A^y/+$ littermates, macrophage infiltration was markedly inhibited by endothelial blockade of NF-κB signaling (Figure 4E). The inhibition of macrophage infiltration was quantitatively confirmed by reverse-transcriptase polymerase chain reaction. Expression of F4/80 and inducible NO synthase was significantly lower in adipose tissues of E-DNIκB;$A^y/+$ mice than in those of control littermate $A^y/+$ mice (Figure 4F). These findings indicate that endothelial NF-κB signaling is involved in obesity-induced macrophage infiltration into adipose tissue. In addition, E-selectin expression was significantly decreased and VCAM-1 and intercel-

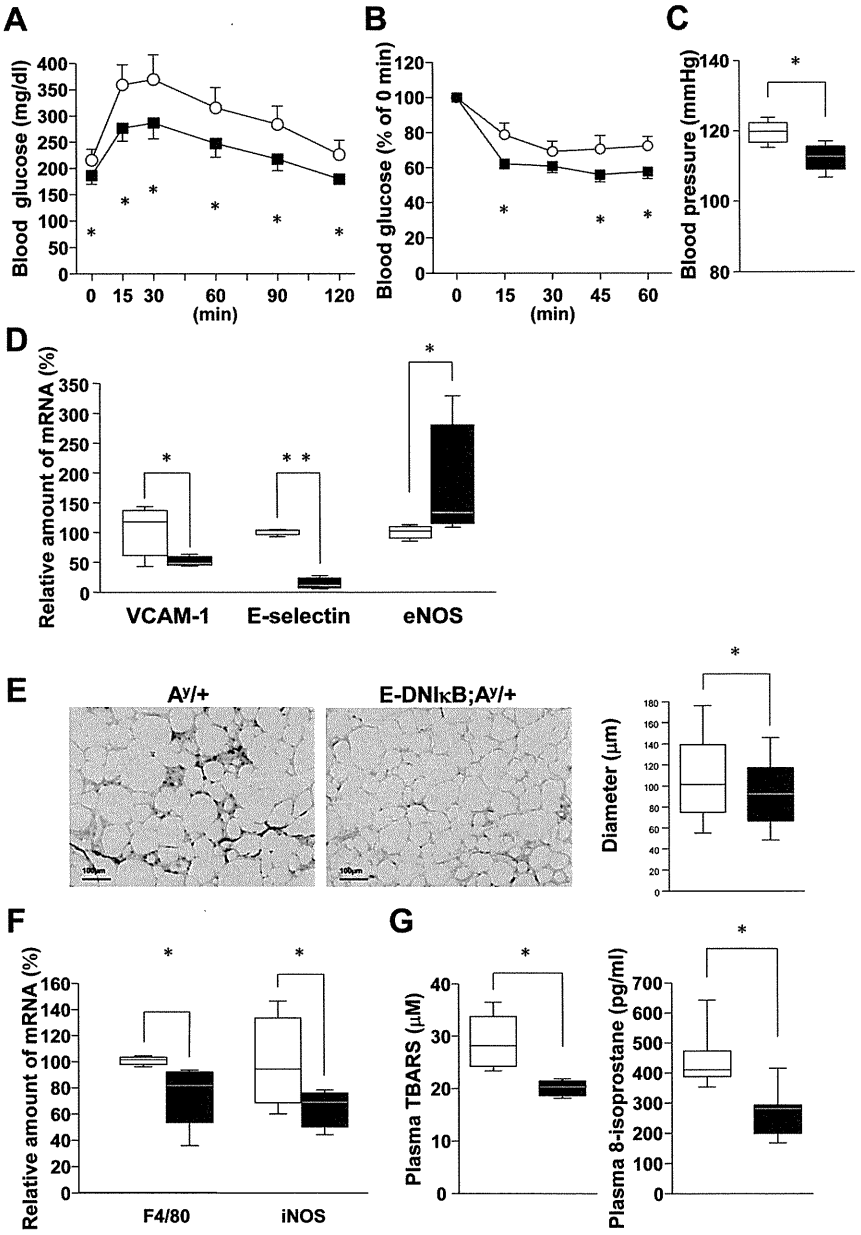

Figure 4. Blockade of endothelial nuclear factor-κB (NF-κB) signaling prevented adipose macrophage infiltration in genetically obese mice. **A**, Male KK A^y (A^y/+) control mice (○) and endothelial dominant-negative IκBα transgenic mice mated with male KK A^y (E-DNIκB;A^y/+; ■) received glucose tolerance tests with a peritoneal glucose load (0.5 g/kg body weight) after a 10-hour fast at 16 weeks of age. **B**, Insulin tolerance tests were performed in an ad libitum–fed state at 16 weeks of age. Data are expressed as percentages of blood glucose levels immediately before intraperitoneal insulin loading (2.5 U/kg body weight). **C**, Systolic blood pressures were measured in A^y/+ control (white bars) and E-DNIκB;A^y/+ (black bars) mice at 16 weeks of age. **D**, Aortic gene expression of vascular cell adhesion molecule-1 (VCAM-1), E-selectin, and endothelial nitric oxide synthase (eNOS) was analyzed in A^y/+ control and E-DNIκB;A^y/+ mice at 16 weeks of age by reverse-transcriptase polymerase chain reaction (RT-PCR). **E**, Epididymal fat from A^y/+ control and E-DNIκB;A^y/+ mice were immunostained with anti-MOMA2 antibody (left). Cell diameters were measured (right). **F**, Gene expression of macrophage markers in epididymal fat was analyzed in A^y/+ control and E-DNIκB;A^y/+ mice by RT-PCR. In **D** and **F**, the relative amounts of mRNA were calculated with β-actin mRNA as the invariant control. **G**, Plasma concentrations of the oxidative stress markers thiobarbituric acid–reactive substance (TBARS) and 8-isoprostane were measured in A^y/+ control and E-DNIκB;A^y/+ mice. Data are presented as mean±SEM. n=5 in A^y/+ control and n=7 in E-DNIκB;A^y/+ mice. *P<0.05 by 1-way repeated-measures ANOVAs and Kruskal-Wallis tests.

lular adhesion molecule-1 tended to be downregulated in adipose tissues of E-DNIκB;A^y/+ mice, whereas angiogenesis markers such as Tie2 and vascular endothelial growth factor did not differ (Figure III in the online-only Data Supplement). Thus, suppression of endothelial expression of adhesion molecules might be involved in the decrease in macrophage infiltration into adipose tissue observed in E-DNIκB;A^y/+ mice.

Plasma leptin, TNF-α, and monocyte chemoattractant protein-1 tended to be lower whereas adiponectin was significantly higher in E-DNIκB;A^y/+ mice than in A^y/+ littermates (Figure IV in the online-only Data Supplement). Furthermore, plasma levels of the oxidative stress markers thiobarbituric acid–reactive substance and 8-isoprostane were significantly lower in E-DNIκB;A^y/+ mice than in A^y/+ littermates (Figure 4G). Aortic expression of the antioxidant enzymes manganese superoxide dismutase and glutathione peroxidase was significantly suppressed in E-DNIκB;A^y/+ mice (Figure V in the online-only Data Supplement), suggesting amelioration of oxidative stress in vascular cells. Taken together, these observations indicate that endothelial NF-κB signaling is involved in obesity-associated inflammation and oxidative stress.

Blood Flow and Mitochondrial Contents Were Increased in Muscles of E-DNIκB;A^y/+ Mice

Endothelial adhesion molecule expression is involved in the leukocyte-endothelium interaction, which reportedly affects the microcirculation.[24] In addition, endothelium-derived NO is widely recognized as a major vasodilator[25] that modulates mitochondrial biogenesis.[26] Because endothelial blockade of NF-κB signaling decreased and increased aortic expression of vascular adhesion molecules and eNOS, respectively (Figure 4D), we first measured blood flow in muscle, a major

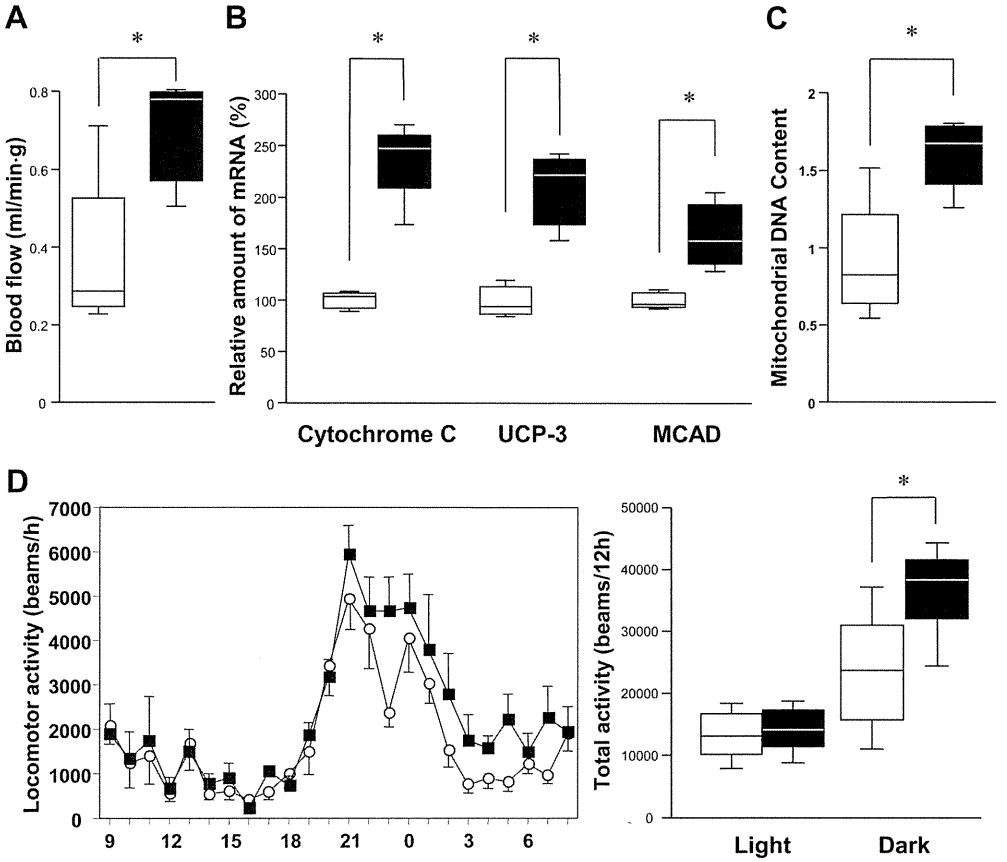

Figure 5. Blood flow and mitochondrial contents were increased in muscles of endothelial dominant-negative IκBα transgenic mice mated with male KK A^y (E-DNIκB;A^y/+) mice. **A**, Gastrocnemius muscle blood flows of 16-week-old A^y/+ control (white bars, n=4) and E-DNIκB;A^y/+ (black bars, n=4) mice were measured with the fluorescent microsphere method. **B**, Gene expression of mitochondrial proteins in muscle was analyzed in A^y/+ control and E-DNIκB;A^y/+ mice by reverse-transcriptase polymerase chain reaction. The relative amounts of mRNA were calculated with α-actin mRNA as the invariant control. UCP-3 indicates uncoupling protein-3; MCAD, medium-chain acyl-CoA dehydrogenase. **C**, Total DNA was extracted from gastrocnemius muscles of A^y/+ control and E-DNIκB;A^y/+ mice, and mitochondrial DNA contents were measured with a sequence detection system. In **B** and **C**, the relative amounts of mRNA were calculated with α-actin mRNA as the invariant control. n=5 in A^y/+ control and n=7 in E-DNIκB;A^y/+ mice. **D**, Locomotor activities at 20 to 24 weeks of age of A^y/+ control (○; n=4) and E-DNIκB;A^y/+ (■; n=4) mice (left). Estimated activities in 12-hour light and dark periods (right) were calculated. Data are presented as mean±SEM. *$P<0.05$ by 1-way ANOVA.

insulin-sensitive tissue, using the fluorescent microsphere method.[18,27] Blockade of endothelial NF-κB signaling significantly increased blood flow in the muscles of A^y/+ mice (Figure 5A), suggesting involvement in the prevention of obesity-induced insulin resistance. Next, we examined mitochondrial protein expression and mitochondrial DNA contents. Mitochondrial proteins such as cytochrome c, uncoupling protein-3, and medium-chain acyl-CoA dehydrogenase were upregulated in muscles of E-DNIκB;A^y/+ mice compared with A^y/+ littermate controls (Figure 5B). Mitochondrial DNA contents were significantly higher in muscles of E-DNIκB;A^y/+ mice (Figure 5C). These findings indicate that blockade of endothelial NF-κB signaling enhances mitochondrial biogenesis in muscle.

Then, we assessed whether locomotor activity was affected by blockade of endothelial NF-κB signaling. Interestingly, E-DNIκB mice exhibited significant increments in locomotor activity during the 12-hour dark phase, whereas locomotor activities did not differ during the 12-hour light phase (Figure 5D). Compatible with this, oxygen consumption was also increased in E-DNIκB mice during the dark phase but unchanged in the light phase (Figure VI in the online-only Data Supplement). Because muscle blood flow[28] and mitochondrial function[29] are reportedly involved in insulin sensitivity, these enhancements associated with increased locomotor activity may underlie the protection from insulin resistance in response to blockade of endothelial NF-κB signaling.

E-DNIκB Mice Were Protected From Age-Related Insulin Resistance and Blood Pressure Elevation

Insulin resistance, elevated blood pressure, and increased oxidative stress, which were prevented in obese E-DNIκB mice, are also commonly observed in aged states. Therefore, we next examined the effects of endothelial NF-κB blockade on age-related metabolic deteriorations and vascular senescence using 50-week-old E-DNIκB mice on a standard chow diet. Food intakes were similar (Figure VIIA in the online-only Data Supplement), but body weights were slightly lower in aged E-DNIκB mice than in wild-type littermates (Figure VIIB in the online-only Data Supplement). Blood glucose levels after glucose loading tended to

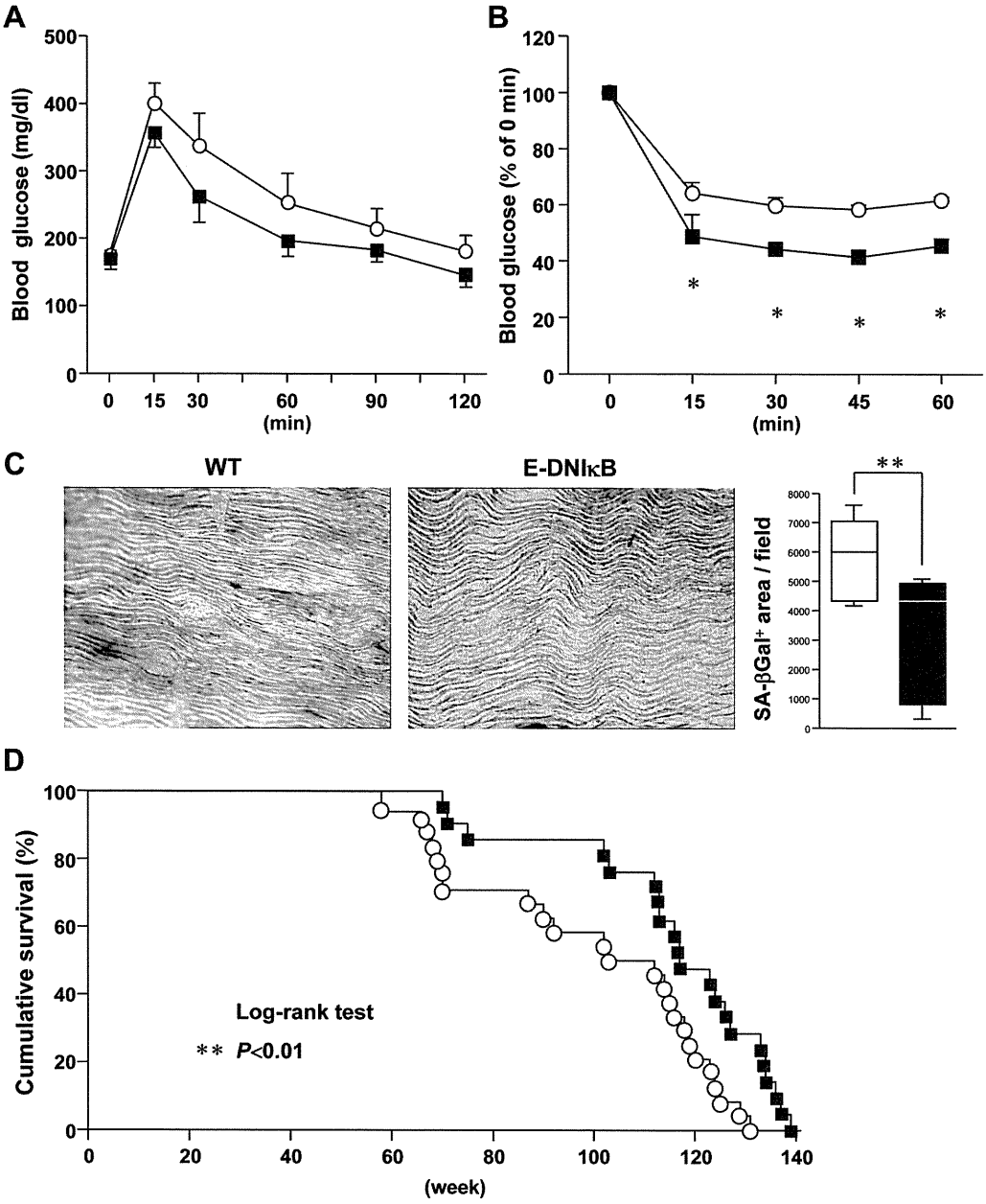

Figure 6. Blockade of nuclear factor-κB (NF-κB) signaling prevented vascular senescence and prolonged life span. **A**, Control (○; n=6) and endothelial dominant-negative IκBα transgenic (E-DNIκB; ■; n=8) mice received glucose tolerance tests with a peritoneal glucose load (1.5 g/kg body weight) after a 10-hour fast at 50 weeks of age. **B**, Insulin tolerance tests were performed in an ad libitum–fed state. Data are expressed as percentages of blood glucose levels immediately before intraperitoneal insulin loading (0.75 U/kg body weight) at 50 weeks of age. **C**, Aortas from aged control and E-DNIκB mice at 90 weeks of age were stained for senescence-associated β-galactosidase (SAβ-gal). SAβ-gal–positive areas of aortas from aged control (white bars, n=5) and E-DNIκB (black bars, n=5) mice were measured (right). Data are presented as mean±SEM. *$P<0.05$, **$P<0.01$ vs control littermate group by 1-way and repeated-measures ANOVA. WT indicates wild type. **D**, Cumulative survival of control (○; n=24) and E-DNIκB (■; n=21) mice on a normal chow diet was analyzed by the Kaplan-Meier method. **$P<0.01$ by the log-rank test.

be lower in E-DNIκB mice, although the differences were not statistically significant (Figure 6A). Insulin tolerance tests revealed better insulin sensitivity in E-DNIκB mice (Figure 6B). Thus, blockade of endothelial NF-κB signaling inhibited the development of age-related insulin resistance.

Furthermore, systolic blood pressure was significantly lower in E-DNIκB mice than in wild-type controls of the same age (Figure VIIIA in the online-only Data Supplement). To determine whether eNOS mediates age-related blood pressure elevation via endothelial NF-κB signaling, we next crossed E-DNIκB mice with eNOS-deficient ($Nos3^{-/-}$) mice. Whereas endothelial DNIκB expression suppressed blood pressure elevation in $Nos3^{+/+}$ mice, eNOS deficiency blunted the inhibitory effects of DNIκB on blood pressure elevation (Figure VIIIA in the online-only Data Supplement). These findings indicate involvement of eNOS in protection from age-related hypertension in E-DNIκB mice.

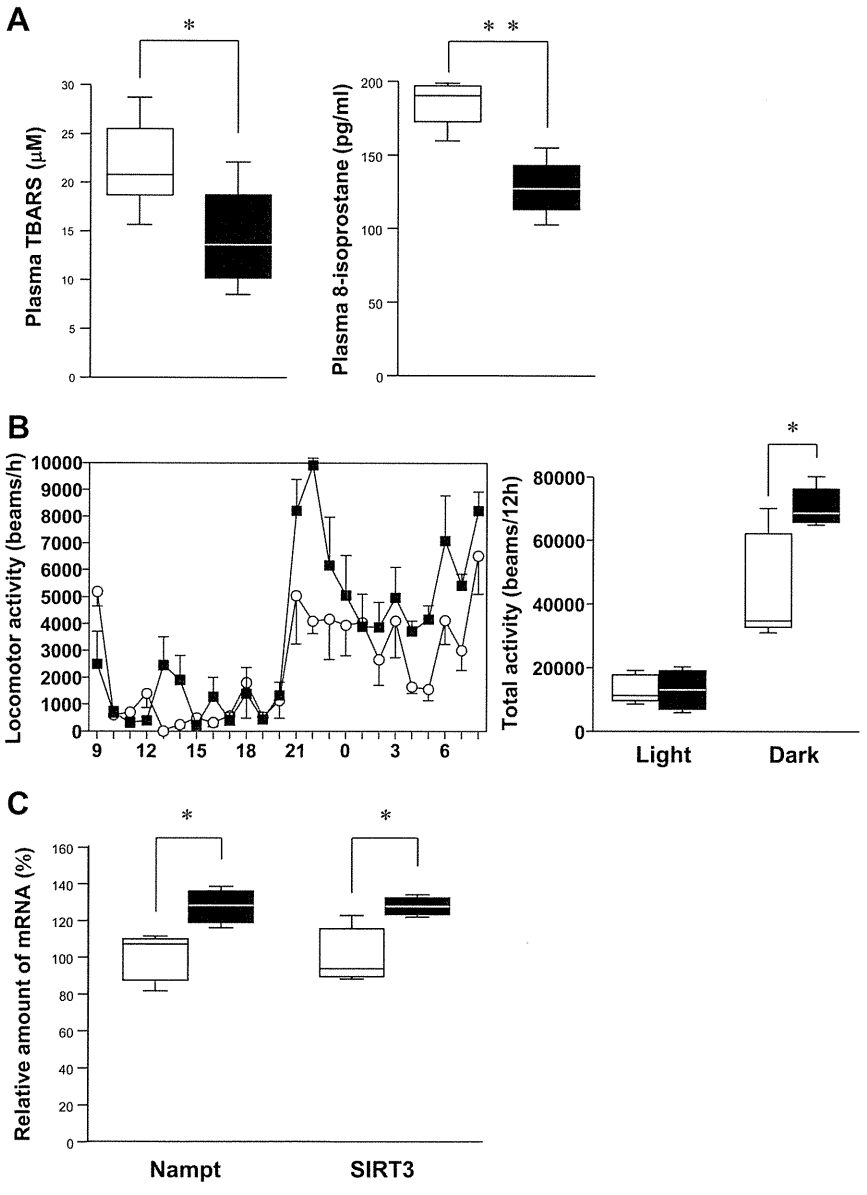

Figure 7. Increments in locomotor activity and upregulation of mitochondrial prosurvival genes in endothelial dominant-negative IκBα transgenic (E-DNIκB)mice. **A**, Plasma thiobarbituric acid–reactive substance (TBARS) and 8-isoprostane concentrations were measured in aged control (white bars, n=6) and E-DNIκB (black bars, n=8) mice at 50 weeks of age. **B**, Locomotor activities of aged control (○; n=5) and E-DNIκB (■; n=5) mice at 50 weeks of age (left). Estimated activities of aged control and E-DNIκB mice in 12-hour light and dark periods (right) were calculated. **C**, Aortic gene expression of mitochondrial prosurvival genes in 50-week-old aged control and E-DNIκB mice was analyzed by reverse-transcriptase polymerase chain reaction. The relative amounts of mRNA were calculated with β-actin mRNA as the invariant control. Data are presented as means±SEM. Nampt indicates nicotinamide phosphoribosyltransferase n=5 in each group. *$P<0.05$, **$P<0.01$ by 1-way ANOVA.

Blockade of NF-κB Signaling Prevented Vascular Senescence and Prolonged Life Span in Mice

Next, we analyzed vascular senescence by β-galactosidase staining of the aortas of aged E-DNIκB mice at 90 weeks of age because endogenous β-galactosidase activity is reportedly increased in senescent states.[20] As shown in Figure 6C, β-galactosidase staining was much weaker in the aortas of E-DNIκB mice, suggesting prevention of vascular senescence by endothelial blockade of NF-κB signaling. These findings prompted us to hypothesize that endothelial NF-κB signaling affects longevity. Therefore, we analyzed the life spans of these mice. E-DNIκB mice and control littermates were fed a standard chow diet ad libitum and maintained in regular housing until death. Intriguingly, E-DNIκB mice exhibited significantly prolonged life spans compared with control littermates ($P=0.0095$ by log-rank test; Figure 6D). Thus, blockade of endothelial NF-κB signaling may prevent age-related metabolic deterioration and vascular senescence and thereby increase longevity.

Similarly in the obesity model, plasma levels of oxidative stress markers were significantly lower in aged E-DNIκB mice at 50 weeks of age than in wild-type controls of the same age (Figure 7A). Blood flow in muscles was increased in aged E-DNIκB mice compared with wild-type littermates, whereas eNOS deficiency blunted the effects of increased blood flow in aged E-DNIκB;Nos3$^{-/-}$ mice (Figure VIIIB in the online-only Data Supplement). Furthermore, blockade of endothelial NF-κB signaling enhanced locomotor activity during the 12-hour dark phase with no significant alterations during the 12-hour light phase (Figure 7B).

Oxidative damage to mitochondria reportedly contributes to aging and various age-related disorders.[30] In human subjects, endurance exercise reportedly enhances mitochondrial SIRT3 expression.[31] Upregulation of nicotinamide phosphoribosyltransferase (Nampt) and SIRT3, which are highly expressed in mitochondria, is linked to life-span extension in the context of caloric restriction.[32] Therefore, we next examined the expression of Nampt and a mitochondrial sirtuin,

SIRT3, in the aortas of 50-week-old E-DNIκB and control mice. In E-DNIκB mice, both Nampt and SIRT3 were actually upregulated (Figure 7C) despite no food intake differences (Figure VIIA in the online-only Data Supplement). Thus, decreased oxidative stress, enhanced active-phase locomotor activity, and upregulation of mitochondrial prosurvival genes might contribute to the life-span prolongation resulting from NF-κB signaling blockade in the endothelium.

Discussion

The endothelium forms an interface between vascular structures and blood. Endothelial cells produce and react to a wide variety of mediators, including cytokines, growth factors, vasoactive substances, and chemokines, as well as adhesion molecules. Therefore, in this study, we focused on proinflammatory responses in the endothelium in an effort to elucidate the role of endothelial NF-κB signaling. We blocked this signaling in vivo by expressing the dominant-negative form of IκBα in endothelial cells using the transgenic procedure. Although E-DNIκB mice displayed no overt phenotypic changes when young and lean, they were protected from the development of both obesity-induced and age-related insulin resistance. Furthermore, intriguingly, E-DNIκB mice were also protected from vascular senescence and showed extended longevity.

The mechanisms underlying protection from obesity-induced insulin resistance in E-DNIκB mice are likely to involve suppression of macrophage infiltration into adipose tissue. Recent studies have demonstrated that macrophage infiltration into white adipose tissues is increased in obesity, raising levels of proinflammatory cytokines such as TNF-α.[22,23] Such macrophage infiltration into adipose tissue may be triggered by the interaction between endothelial cells and macrophages via adhesion molecules. The expression of adhesion molecules is reportedly regulated by NF-κB in the endothelium.[33] In the present study, the expression of vascular adhesion molecules was actually decreased in E-DNIκB mice. A series of recent reports have indicated angiogenic factors to be involved in the development of obesity in adipose tissue.[34] However, adipose expression of Tie2 and vascular endothelial growth factor did not differ between E-DNIκB;Ay/+ mice and control Ay/+ littermates, suggesting minimal effects of endothelial NF-κB signaling on angiogenesis in adipose tissue. In addition, proinflammatory cytokines secreted by macrophages in adipose tissue may further activate the endothelial NF-κB pathway, producing a deleterious cycle. Indeed, epididymal fat weight was significantly lower and plasma adiponectin was higher in E-DNIκB;Ay/+ mice than in Ay/+ littermates. Therefore, interruption of this deleterious cycle by blockade of endothelial NF-κB signaling is speculated to contribute to protection from obesity-related chronic inflammation and increased oxidative stress in E-DNIκB mice.

Decreased eNOS production may lead to a reduction in microcirculatory blood flow and elevated blood pressure. Endothelium-derived NO is a major vasodilator,[35] and constitutive NO production by endothelial cells reportedly inhibits adhesion molecule expression through stabilization of IκB.[36] On the other hand, in this study, eNOS expression was enhanced in E-DNIκB mice, suggesting that endothelial NF-κB signaling per se negatively regulates eNOS expression. Furthermore, in $NOS3^{-/-}$ mice, endothelial DNIκB expression did not significantly suppress age-related hypertension or increase blood flow in muscle, indicating the involvement of eNOS in the antihypertensive effects of endothelial NF-κB blocking. NO production and NF-κB activation affect each other in endothelial cells. NF-κB activation decreases eNOS expression, resulting in decreased NO production and thus further NF-κB activation, producing a vicious cycle that further decreases microcirculation and increases proinflammatory responses and oxidative stress. The attenuation of microcirculatory blood flow observed in eNOS-deficient mice decreases transcapillary passage of insulin to metabolically active tissues such as muscle, thereby contributing to impairment of insulin action.[18] Negative regulation of eNOS expression by NF-κB in endothelial cells is thus another important mechanism underlying insulin resistance and hypertension.

Insulin resistance, elevated blood pressure, and increased oxidative stress are commonly observed not only in obese but also in aged states. These age-related metabolic deteriorations were also prevented in E-DNIκB mice, in association with increased muscle blood flow and decreased oxidative stress markers. Furthermore, it is noteworthy that E-DNIκB mice were protected from vascular senescence and lived longer even under normal chow-fed conditions. At the cellular level, NF-κB has been implicated in age-dependent induction of cellular senescence.[37] However, in this study, blockade of NF-κB signaling selectively in endothelial cells affected vascular senescence of the whole aorta and the life spans of the model animals. Therefore, intracellular events in the endothelium alone cannot explain these antiaging phenotypes manifesting in the whole body. Relatively early deaths of E-DNIκB mice (60–100 weeks of age) were decreased and maximum life span was longer in E-DNIκB mice, suggesting that endothelial NF-κB blockade prevents both fatal morbidities and senescence. Amelioration of insulin resistance and decreased oxidative stress likely contribute to these systemic antiaging phenotypes.

In addition, mitochondrial function may be involved in the underlying mechanism. Mitochondrial dysfunction in muscle promotes the development of insulin resistance in obese[29] and aged[38] human subjects and contributes to aging and various age-related disorders.[30] Mitochondrial dysfunction is also linked to decreased muscle blood flow with aging.[39] Because eNOS reportedly modulates mitochondrial biogenesis,[26] eNOS upregulation may contribute to enhanced mitochondrial contents in muscles of E-DNIκB mice. Furthermore, endurance exercise, which is considered to confer life-span–extending effects, enhances the expression of a mitochondrial sirtuin, SIRT3, in human subjects.[31] SIRT3 was initially reported to be linked to caloric restriction–induced cell survival.[40,41] Nampt provides mitochondrial NAD+ as the cosubstrate for SIRT3, and enhanced Nampt and SIRT3 expression maintains mitochondrial viability and promote cell survival.[42] In the present study, aortic expression of Nampt and SIRT3 was significantly upregulated in aged

E-DNIκB mice, suggesting contributions of the sirtuin pathway to the antisenescence and prolonged longevity phenotypes. Thus, various mechanisms derived from endothelial NF-κB signaling, including systemic locomotion, systemic oxidative stress, peripheral blood flow, and mitochondrial sirtuins, may influence longevity in a complex manner (Figure IX in the online-only Data Supplement).

It was recently reported that global disruption of the angiotensin II type 1 receptor promotes longevity.[43] In these knockout mice as well, Nampt and SIRT3 were upregulated in the kidney. The angiotensin II type 1 receptor pathway activates a variety of intracellular signaling pathways, including NF-κB signaling.[44] However, although a growing body of evidence for angiotensin II signaling in smooth muscle cells has accumulated, much less is known about endothelial angiotensin II signal transduction and function.[45] The present study suggests the specific importance of NF-κB signaling in endothelial cells for the mechanism underlying the life-span extension observed in globally angiotensin II type 1 receptor–deficient mice. Although further intensive studies are necessary to elucidate the precise mechanisms, the endothelium apparently plays important roles in determining life span.

Adhesion molecule expression in the endothelium is well known to promote atherosclerotic plaque formation.[46] Indeed, blockade of endothelial NF-κB signaling suppresses hypercholesterolemia-induced atherosclerosis caused by apolipoprotein E deficiency.[47] Therefore, endothelial NF-κB signaling is apparently involved in the development of obesity-related disorders, including insulin resistance, hypertension, and atherosclerosis, via a variety of processes in different tissues. Furthermore, in this study, selective blockade of endothelial NF-κB signaling not only prevented age-related insulin resistance but also inhibited senescence and increased longevity with normal chow feeding. Thus, endothelial NF-κB signaling is a potential target for treatment of the metabolic syndrome and for antiaging strategies.

Acknowledgments

We thank Dr Thomas N. Sato for the generous gift of a vector containing the Tie2 promoter and enhancer. We are indebted to M. Hoshi, I. Sato, T. Takasugi, and J. Fushimi, who assisted in various aspects of this study.

Sources of Funding

This work was supported by Grants-in-Aid for Scientific Research (15390282) to Dr Katagiri and (22790681) to Dr Hasegawa from the Japan Society for the Promotion of Science of Japan. This work was also supported by a Grant-in-Aid for Scientific Research on Innovative Areas (to Dr Katagiri) and the Global-COE (to Drs Katagiri and Oka) from the Ministry of Education, Culture, Sports, Science, and Technology of Japan.

Disclosures

None.

References

1. Hayden MS, Ghosh S. Shared principles in NF-kappaB signaling. *Cell*. 2008;132:344–362.
2. Karin M, Yamamoto Y, Wang QM. The IKK NF-kappa B system: a treasure trove for drug development. *Nat Rev Drug Discov*. 2004;3:17–26.
3. Hotamisligil GS. Inflammation and metabolic disorders. *Nature*. 2006;444:860–867.
4. Semenkovich CF. Insulin resistance and atherosclerosis. *J Clin Invest*. 2006;116:1813–1822.
5. Alberti KG, Zimmet P, Shaw J. The metabolic syndrome: a new worldwide definition. *Lancet*. 2005;366:1059–1062.
6. Katagiri H, Yamada T, Oka Y. Adiposity and cardiovascular disorders: disturbance of the regulatory system consisting of humoral and neuronal signals. *Circ Res*. 2007;101:27–39.
7. Arkan MC, Hevener AL, Greten FR, Maeda S, Li ZW, Long JM, Wynshaw-Boris A, Poli G, Olefsky J, Karin M. IKK-beta links inflammation to obesity-induced insulin resistance. *Nat Med*. 2005;11:191–198.
8. Yuan M, Konstantopoulos N, Lee J, Hansen L, Li ZW, Karin M, Shoelson SE. Reversal of obesity- and diet-induced insulin resistance with salicylates or targeted disruption of IKKbeta. *Science*. 2001;293:1673–1677.
9. Kim JK, Kim YJ, Fillmore JJ, Chen Y, Moore I, Lee J, Yuan M, Li ZW, Karin M, Perret P, Shoelson SE, Shulman GI. Prevention of fat-induced insulin resistance by salicylate. *J Clin Invest*. 2001;108:437–446.
10. Aird WC. Phenotypic heterogeneity of the endothelium, I: structure, function, and mechanisms. *Circ Res*. 2007;100:158–173.
11. Rocha VZ, Libby P. Obesity, inflammation, and atherosclerosis. *Nat Rev Cardiol*. 2009;6:399–409.
12. Kim JA, Montagnani M, Koh KK, Quon MJ. Reciprocal relationships between insulin resistance and endothelial dysfunction: molecular and pathophysiological mechanisms. *Circulation*. 2006;113:1888–1904.
13. Hasegawa Y, Ogihara T, Yamada T, Ishigaki Y, Imai J, Uno K, Gao J, Kaneko K, Ishihara H, Sasano H, Nakauchi H, Oka Y, Katagiri H. Bone marrow (BM) transplantation promotes beta-cell regeneration after acute injury through BM cell mobilization. *Endocrinology*. 2007;148:2006–2015.
14. Imai J, Katagiri H, Yamada T, Ishigaki Y, Suzuki T, Kudo H, Uno K, Hasegawa Y, Gao J, Kaneko K, Ishihara H, Niijima A, Nakazato M, Asano T, Minokoshi Y, Oka Y. Regulation of pancreatic beta cell mass by neuronal signals from the liver. *Science*. 2008;322:1250–1254.
15. Marelli-Berg FM, Peek E, Lidington EA, Stauss HJ, Lechler RI. Isolation of endothelial cells from murine tissue. *J Immunol Methods*. 2000;244:205–215.
16. Uno K, Katagiri H, Yamada T, Ishigaki Y, Ogihara T, Imai J, Hasegawa Y, Gao J, Kaneko K, Iwasaki H, Ishihara H, Sasano H, Inukai K, Mizuguchi H, Asano T, Shiota M, Nakazato M, Oka Y. Neuronal pathway from the liver modulates energy expenditure and systemic insulin sensitivity. *Science*. 2006;312:1656–1659.
17. Iwamoto T, Kita S, Zhang J, Blaustein MP, Arai Y, Yoshida S, Wakimoto K, Komuro I, Katsuragi T. Salt-sensitive hypertension is triggered by Ca^{2+} entry via Na^{+}/Ca^{2+} exchanger type-1 in vascular smooth muscle. *Nat Med*. 2004;10:1193–1199.
18. Kubis N, Richer C, Domergue V, Giudicelli JF, Levy BI. Role of microvascular rarefaction in the increased arterial pressure in mice lacking for the endothelial nitric oxide synthase gene (eNOS3pt−/−). *J Hypertens*. 2002;20:1581–1587.
19. Gao J, Katagiri H, Ishigaki Y, Yamada T, Ogihara T, Imai J, Uno K, Hasegawa Y, Kanzaki M, Yamamoto TT, Ishibashi S, Oka Y. Involvement of apolipoprotein E in excess fat accumulation and insulin resistance. *Diabetes*. 2007;56:24–33.
20. Kunieda T, Minamino T, Nishi J, Tateno K, Oyama T, Katsuno T, Miyauchi H, Orimo M, Okada S, Takamura M, Nagai T, Kaneko S, Komuro I. Angiotensin II induces premature senescence of vascular smooth muscle cells and accelerates the development of atherosclerosis via a p21-dependent pathway. *Circulation*. 2006;114:953–960.
21. Kim I, Moon SO, Kim SH, Kim HJ, Koh YS, Koh GY. Vascular endothelial growth factor expression of intercellular adhesion molecule 1 (ICAM-1), vascular cell adhesion molecule 1 (VCAM-1), and E-selectin through nuclear factor-kappa B activation in endothelial cells. *J Biol Chem*. 2001;276:7614–7620.
22. Xu H, Barnes GT, Yang Q, Tan G, Yang D, Chou CJ, Sole J, Nichols A, Ross JS, Tartaglia LA, Chen H. Chronic inflammation in fat plays a crucial role in the development of obesity-related insulin resistance. *J Clin Invest*. 2003;112:1821–1830.
23. Weisberg SP, McCann D, Desai M, Rosenbaum M, Leibel RL, Ferrante AW Jr. Obesity is associated with macrophage accumulation in adipose tissue. *J Clin Invest*. 2003;112:1796–1808.
24. Nishimura S, Manabe I, Nagasaki M, Seo K, Yamashita H, Hosoya Y, Ohsugi M, Tobe K, Kadowaki T, Nagai R, Sugiura S. In vivo imaging in

mice reveals local cell dynamics and inflammation in obese adipose tissue. *J Clin Invest.* 2008;118:710–721.
25. Huang PL, Huang Z, Mashimo H, Bloch KD, Moskowitz MA, Bevan JA, Fishman MC. Hypertension in mice lacking the gene for endothelial nitric oxide synthase. *Nature.* 1995;377:239–242.
26. Nisoli E, Clementi E, Paolucci C, Cozzi V, Tonello C, Sciorati C, Bracale R, Valerio A, Francolini M, Moncada S, Carruba MO. Mitochondrial biogenesis in mammals: the role of endogenous nitric oxide. *Science.* 2003;299:896–899.
27. Gervais M, Demolis P, Domergue V, Lesage M, Richer C, Giudicelli JF. Systemic and regional hemodynamics assessment in rats with fluorescent microspheres. *J Cardiovasc Pharmacol.* 1999;33:425–432.
28. Duplain H, Burcelin R, Sartori C, Cook S, Egli M, Lepori M, Vollenweider P, Pedrazzini T, Nicod P, Thorens B, Scherrer U. Insulin resistance, hyperlipidemia, and hypertension in mice lacking endothelial nitric oxide synthase. *Circulation.* 2001;104:342–345.
29. Lowell BB, Shulman GI. Mitochondrial dysfunction and type 2 diabetes. *Science.* 2005;307:384–387.
30. Chan DC. Mitochondria: dynamic organelles in disease, aging, and development. *Cell.* 2006;125:1241–1252.
31. Lanza IR, Short DK, Short KR, Raghavakaimal S, Basu R, Joyner MJ, McConnell JP, Nair KS. Endurance exercise as a countermeasure for aging. *Diabetes.* 2008;57:2933–2942.
32. Lin SJ, Kaeberlein M, Andalis AA, Sturtz LA, Defossez PA, Culotta VC, Fink GR, Guarente L. Calorie restriction extends *Saccharomyces cerevisiae* lifespan by increasing respiration. *Nature.* 2002;418:344–348.
33. De Martin R, Hoeth M, Hofer-Warbinek R, Schmid JA. The transcription factor NF-kappa B and the regulation of vascular cell function. *Arterioscler Thromb Vasc Biol.* 2000;20:E83–E88.
34. Cao Y. Angiogenesis modulates adipogenesis and obesity. *J Clin Invest.* 2007;117:2362–2368.
35. Palmer RM, Ferrige AG, Moncada S. Nitric oxide release accounts for the biological activity of endothelium-derived relaxing factor. *Nature.* 1987; 327:524–526.
36. Peng HB, Libby P, Liao JK. Induction and stabilization of I kappa B alpha by nitric oxide mediates inhibition of NF-kappa B. *J Biol Chem.* 1995; 270:14214–14219.
37. Adler AS, Kawahara TL, Segal E, Chang HY. Reversal of aging by NFkappaB blockade. *Cell Cycle.* 2008;7:556–559.
38. Petersen KF, Befroy D, Dufour S, Dziura J, Ariyan C, Rothman DL, DiPietro L, Cline GW, Shulman GI. Mitochondrial dysfunction in the elderly: possible role in insulin resistance. *Science.* 2003;300:1140–1142.
39. Terjung RL, Zarzeczny R, Yang HT. Muscle blood flow and mitochondrial function: influence of aging. *Int J Sport Nutr Exerc Metab.* 2002;12:368–378.
40. Sinclair DA, Lin SJ, Guarente L. Life-span extension in yeast. *Science.* 2006;312:195–197.
41. Lin SJ, Defossez PA, Guarente L. Requirement of NAD and SIR2 for life-span extension by calorie restriction in *Saccharomyces cerevisiae.* *Science.* 2000;289:2126–2128.
42. Yang H, Yang T, Baur JA, Perez E, Matsui T, Carmona JJ, Lamming DW, Souza-Pinto NC, Bohr VA, Rosenzweig A, de Cabo R, Sauve AA, Sinclair DA. Nutrient-sensitive mitochondrial NAD+ levels dictate cell survival. *Cell.* 2007;130:1095–1107.
43. Benigni A, Corna D, Zoja C, Sonzogni A, Latini R, Salio M, Conti S, Rottoli D, Longaretti L, Cassis P, Morigi M, Coffman TM, Remuzzi G. Disruption of the Ang II type 1 receptor promotes longevity in mice. *J Clin Invest.* 2009;119:524–530.
44. Li XC, Zhuo JL. Nuclear factor-kappaB as a hormonal intracellular signaling molecule: focus on angiotensin II-induced cardiovascular and renal injury. *Curr Opin Nephrol Hypertens.* 2008;17:37–43.
45. Higuchi S, Ohtsu H, Suzuki H, Shirai H, Frank GD, Eguchi S. Angiotensin II signal transduction through the AT1 receptor: novel insights into mechanisms and pathophysiology. *Clin Sci.* 2007;112:417–428.
46. Ross R. Atherosclerosis: an inflammatory disease. *N Engl J Med.* 1999; 340:115–126.
47. Gareus R, Kotsaki E, Xanthoulea S, van der Made I, Gijbels MJ, Kardakaris R, Polykratis A, Kollias G, de Winther MP, Pasparakis M. Endothelial cell-specific NF-kappaB inhibition protects mice from atherosclerosis. *Cell Metab.* 2008;8:372–383.

CLINICAL PERSPECTIVE

Insulin resistance is an important mechanism underlying obesity-related disorders, eg, diabetes, hyperlipidemia, and hypertension, collectively called the metabolic syndrome. In particular, inflammation and oxidative stress are well known to play important roles in the pathogenesis of this systemic syndrome and the resultant development of atherosclerosis. A transcription factor, nuclear factor-κB (NF-κB), has been considered to mediate the responses to both inflammation and oxidative stress intracellularly. However, the site(s) at which the NF-κB signaling pathway plays critical roles in these pathological processes remains to be elucidated. This study focused on the roles of endothelial NF-κB signaling. By expressing the dominant-negative IκB mutant in the endothelium using the transgenic procedure, the NF-κB signaling pathway was blocked selectively in endothelial cells. These mice were protected from the development of both obesity- and age-related insulin resistance. Furthermore, importantly, these mice exhibited prolonged lifespans. In addition to the decrease in relatively early deaths, maximum lifespan was shown to be longer in these transgenic mice. Vascular senescence was markedly inhibited by blockade of endothelial NF-κB. Thus, the endothelium plays important roles in obesity- and age-related disorders through intracellular NF-κB signaling, ultimately impacting lifespan. Blockade of endothelial NF-κB signaling apparently protects the whole body from both fatal morbidities at earlier ages and the development of senescence. Amelioration of insulin resistance and decreased oxidative stress are likely to contribute to these beneficial phenotypes. Therefore, endothelial NF-κB signaling is a potential target not only for treating the metabolic syndrome, but also for anti-aging strategies.

SUPPLEMENTAL MATERIAL

Supplemental Methods

Animals

Animal studies were conducted in accordance with the institutional guidelines for animal experiments at Tohoku University. The animals were housed in an air-conditioned environment, with a 12-h light-dark cycle, and fed a regular unrestricted diet or a high-fat diet consisting of 15.3% (wt/wt) fat (Quick Fat; Nippon CLEA, Shizuoka, Japan) starting at 8 weeks of age. The mutant cDNA for human IκBα , with alanine substitutions of two serine residues (32 and 36), was cloned into a transgenic vector, pSPTg.T2FpAXK, provided by Thomas N. Sato. This vector contains the Tie2 promoter, SV40 polyA signal and Tie2 minimum enhancer fragment. To generate transgenic mice, the construct cDNA was linearized with Sal1 digestion and microinjected into fertilized oocytes by Oriental Yeast Co. Genotyping was performed by PCR of tail DNA using the primers 5'-CCATGCGAGCGGGAAGTC-3' and 3'-CGGAGCTCAGGATCACA-5'. The two lines of transgenic mice used in the experiment had similar phenotypes. Founder mice were backcrossed for at least 6 generations with C57BL/6J mice (The Jackson Laboratory, ME, USA). E-DNIκB;A^y/+ mice were obtained by mating male KK A^y (A^y/+) mice (Nippon CLEA, Shizuoka, Japan), a genetic model for obesity-diabetes syndrome, and female E-DNIκB mice. Male E-DNIκB Tg/+: A^y/+ and littermate control male A^y/+ mice were used in the experiment. E-DNIκB mice were crossed with endothelial nitric oxide synthase (eNOS)-deficient ($Nos3^{-/-}$) mice with the C57BL/6J background[1] (The Jackson Laboratory, ME, USA) to generate E-DNIκB;$Nos3^{-/-}$ mice. Littermate $Nos3^{-/-}$ mice were used as controls in these experiments.

Blood analysis

Blood glucose was determined as described previously.[2] Plasma TBARS and 8-isoprostane levels were measured with Assay Kits (Cayman Chemical Co, MN, USA).

Glucose and insulin tolerance tests

Glucose and insulin tolerance tests were performed as described previously.[3] Glucose tolerance tests were performed on fasted (10 h) mice. Mice were injected with glucose into the intraperitoneal space, and blood glucose was assayed immediately before and at 15, 30, 60, 90 and 120 min postadministration. Insulin tolerance tests were performed on fed mice. Mice were injected with human regular insulin (Eli Lilly, Kobe, Japan), and blood glucose was assayed immediately before and at 15, 30, 45 and 60 min postinjection.

Hyperinsulinemic-euglycemic clamp

Hyperinsulinemic-euglycemic clamp studies were performed as described previously.[4] Chronically cannulated, conscious and unrestrained mice were fasted for 6 h before the study. Insulin (500 mU $\cdot$ kg^{-1} $\cdot$ min^{-1}) was infused throughout the clamp study. Blood glucose was monitored every 5 min via carotid arterial catheter samples. Glucose was infused at a variable rate to maintain blood glucose at 120 mg/dl. The glucose infusion rate was calculated as described previously.[4]

Histological analysis

Tissues sections were removed, fixed with 10% formalin, and embedded in paraffin. The streptavidin–biotin (SAB) method was performed using a Histofine SAB-PO kit